ARTICLE

Synthesis of Mesoporous Alumina from Boehmite in the Presence of Triblock Copolymer

Pasquale F. Fulvio, Reno I. Brosey, and Mietek Jaroniec*

Department of Chemistry, Kent State University, Kent, Ohio 44242

ABSTRACT Mesoporous alumina was synthesized using commercial boehmite in the presence of poly(ethylene oxide)-poly(propylene oxide)-poly(ethylene oxide) triblock copolymer Pluronic P123. Its calcination at 400°C yielded γ-alumina, in contrast to the ordered mesoporous alumina (OMA) obtained by hydrolysis of aluminum alkoxide in the presence of the same triblock copolymer. This synthesis afforded boehmite-based mesoporous alumina (BMA) with better adsorption properties and higher thermal stability in comparison to the alkoxide-based OMA, which remained amorphous after calcination below 900°C. The BMA materials also exhibited higher amount of acidic and basic sites as evidenced by ammonia (NH_3) and carbon dioxide (CO_2) temperature programmed desorption (TPD), respectively. Dispersion of commercial boehmite precursor under microwave irradiation afforded BMA materials with similar surface characteristics as those of the corresponding BMA samples obtained under conventional conditions, but showing slightly lower acidity and better basic properties. Thus, the dispersion method of boehmite can be used to modify the surface properties of the resulting BMA samples without sacrificing their porosity.

KEYWORDS: boehmite • acidity • γ -alumina • mesoporous alumina • nitrogen adsorption • temperature programmed desorption

INTRODUCTION

There is a great interest in mesoporous alumina (MA) catalysts having high surface area, large mesopores, crystalline pore walls, and good thermal stability (1−3). To obtain MA, ionic and non-ionic surfactants have been used as structure-directing agents (4). So far, the reported MA samples often have small mesopores and low pore volumes. MAs with large and ordered mesopores have been synthesized via evaporation induced self-assembly (EISA) using aluminum alkoxides and triblock copolymers such as poly(ethylene oxide)-poly(propylene oxide)-poly(ethylene oxide) (PEO-PPO-PEO) (5, 6). Despite the ordered arrangement of pores, these materials exhibited smaller crystallinity and lower thermal stability, whereas their formation occurred under strictly controlled conditions. The use of ordered mesoporous carbons as hard templates resulted in ordered aluminas with better crystallinity, but with narrow mesopores; also, this route required additional steps for the preparation of carbon templates (7). The use of strongly acidic conditions during self-assembly resulted in major improvement of long-range ordering of mesopores for MAs and MA-based mixed oxides (8, 9). This route was recently extended to the preparation of monoliths with hierarchical pore structure using triblock copolymers and polyurethane foam as a co-template (10). The final materials exhibited larger mesopores than those prepared by using hard templates, but their pore walls remained amorphous after calcination in the range of 400−800 °C, whereas the γ-Al_2O_3 phase was observed between 800 and 1000 °C, with transition to nonporous α-Al_2O_3 at 1100 °C.

Nanocrystalline aluminas were reported for different alumina precursors and surfactant templates. For instance, some syntheses employing alkaline hydrolysis of aluminum alkoxides or salts (11, 11−19), aluminate salts (17, 20), polyoxocations (17, 20), and boehmite (21, 22) resulted in the samples with disordered mesopores but showing γ-Al_2O_3 nanocrystalline domains after calcination at 400 °C and good thermal stability. In the most cases, the hydrolysis of aluminum species involved the formation of pseudoboehmite-surfactant nanocomposites that upon thermal treatment were converted to the mesoporous γ-Al_2O_3 phases (8). Even though the direct self-assembly of boehmite sols with triblock copolymers resulted in the samples with disordered textural mesopores, the latter materials also exhibited better thermal stability than the samples prepared from other alumina precursors (21). Boehmite is also a major raw material in industry, largely used for the preparation of alumina catalysts and supports (1−3). Thus, the synthesis of MA from this precursor is of great importance. So far, only aqueous synthesis in the presence of triblock copolymers has been reported, using relatively large acid/aluminum molar ratios ($[H^+]/[Al^{3+}] = 0.3-3.0$), large amounts of water and long synthesis time (21, 22).

Here we report the block copolymer-assisted synthesis of MA in water−ethanol medium using commercial boehmite powder. The resulting MA samples showed improved adsorption properties, much better crystallinity, and higher acidity than ordered mesoporous aluminas (OMAs) prepared by the self-assembly of alkoxides and triblock copolymers.

* Corresponding author. Phone: (330) 672-3790. Fax: (330) 672-3816. E-mail: jaroniec@kent.edu.

Received for review December 16, 2009 and accepted January 27, 2010

DOI: 10.1021/am9009023

Published on Web 02/05/2010

Also, the thermal and chemical stability of boehmite-based MAs (BMAs) is higher than that of the aforementioned OMAs calcined at the same temperatures.

EXPERIMENTAL SECTION

Synthesis of BMAs. Typical synthesis of boehmite-based alumina samples was as follows: 1.20 g of boehmite powder (Catapal A, Sasol) was dispersed in 15 or 20ml of water acidified with 0.13ml of concentrated nitric acid ($[H^+]/[Al^{3+}] = 0.1$) at 70°C for 1 h under conventional heating or microwave irradiation. The resulting sol was transferred to the polymer solution obtained by dissolving Pluronic P123 in 15 or 20 mL of ethanol (200 proof) for at least 2 h at room temperature. The boehmite dispersion and polymer solution were mixed for 5 h. For some materials, an additional 0.13 mL of concentrated nitric acid was added to the boehmite-P123 mixture to obtain $[H^+]/[Al^{3+}] = 0.2$. The gels were allowed to dry in an oven at 60 or 80 °C for 72 h when the total volume of solution was 30 mL and for 48 h when the total volume of solution was 40 mL.

The synthesis of ordered mesoporous aluminas (OMA) was carried out according to the procedure reported by Q. Yuan et al. (8). In a typical synthesis, about 2.00 g of Pluronic P123 (BASF, EO_{20}-PO_{70}-EO_{20}) was dissolved in 20 mL of ethanol (200 proof) at room temperature for 2 h. Approximately 1.00 g of aluminum isopropoxide (Acrós Organics) was added to the polymer solution, followed by addition of 3.2 mL of concentrated nitric acid and 20 mL of ethanol (200 proof). The resulting gel was stirred at room temperature for 5 h and next the solvent was allowed to evaporate in an oven at 60 °C for 72 h.

All composites materials were calcined at 400, 700, or 900 °C for 4 h in flowing air using 1 °C min^{-1} heating rate to reach the specified temperature. Some samples were also calcined in air at 400 °C for 4 h followed by heating at 1100 °C for 1 h using 1 °C min^{-1} and 2 °C min^{-1} heating rates, respectively, to reach the aforementioned temperatures.

Ordered mesoporous aluminas were labeled as OMA-T, where T stands for the calcination temperature of 400, 700, 900, and 1100°C. The boehmite-based mesoporous aluminas were labeled as Bh/*y*-*z*-*x*/T, where Bh stands for boehmite, *y* is the acid to alumina molar ratio (0.1 or 0.2), *z* is the drying temperature (60 or 80°C), *x* is the volume of the solution used (low volume, LV, regular volume, RV, or regular volume under microwave conditions, MW) and T is the calcination temperature.

Two reference samples were prepared without the use of triblock copolymer by dispersing boehmite under the aforementioned conditions in water and $[H^+]/[Al^{3+}] = 0.1$, followed by drying at 60 °C for 12 h. These as-recrystallized samples were calcined under the same conditions as those used for the polymer-assisted synthesis of BMA; these samples were labelled as Bh/0.1-AR-T (conventional heating) or Bh/0.1-MW-T (microwave heating).

Characterization. Nitrogen adsorption isotherms were measured at −196 °C using ASAP 2010 and 2020 volumetric adsorption analyzers manufactured by Micromeritics (Norcross, GA). Before adsorption measurements, the calcined alumina samples were degassed under a vacuum for at least 2 h at 200 °C. The specific surface area of the samples was calculated using the Brunauer−Emmett−Teller (BET) method within the relative pressure range of 0.05−0.20 (23). Pore size distributions were calculated using the BJH algorithm for cylindrical pores according to the KJS method (24, 25) calibrated for pores up to 19 nm.

The wide-angle XRD measurements were conducted for the calcined samples using a PANanalytical, Inc. X'Pert Pro (MPD) Multi Purpose Diffractometer with Cu Kα radiation (1.5406 Å), an operating voltage of 40 kV, 0.020° step size, 3 s step time, and $10.0° < 2\theta < 80.0°$ range at room temperature.

The TG measurements were performed on a TA Instruments TGA 2950 thermogravimetric analyzer using a high-resolution mode. The curves were recorded in flowing air with a heating rate of 10 °C min^{-1} up to 800 °C.

The NH_3 and CO_2-TPD experiments were performed using a Micromeritics Auto Chem II Chemisorption Analyzer (Norcross, GA)) equipped with a thermocouple detector (TCD). Approximately 0.20 g of each sample were loaded in a quartz tube micro-reactor supported by quartz wool and degassed at 500 °C for 1 h before NH_3 and for 2 h before CO_2 using a heating rate of 5 °C min^{-1} in flowing He (50 cm^3 min^{-1}). Next, the samples were cooled to 180 °C and exposed to flowing 5% NH_3−He (50 cm^3 min^{-1}) for 1 h and finally purged in flowing He for 1 h; however, CO_2 chemisorption was done at 120 °C. In the TPD experiments, the samples were heated to 500 °C using 10 °C min^{-1} heating rate and kept at this temperature for 30 min in the case of NH_3 or to 750 °C and kept at the latter temperature for 60 min in the case of CO_2. The amounts of desorbed NH_3 and CO_2 were obtained by integration of the desorption profiles and referenced to the TCD signals calibrated for known volumes of analysis gases.

For scanning electron microscopy analysis (SEM), the samples were manually ground using Agatha mortar, mounted on graphite tape and carbon coated using SPI Module carbon coater. The SEM images were obtained with help of a Hitachi S-4300 field emission SEM (FE-SEM) at an accelerating voltage of 2−5 kV and 350−45 000× magnifications.

RESULTS AND DISCUSSION

The powder XRD patterns of dispersed boehmite precursors are shown in Figure 1 A. After dispersion of boehmite in aqueous solution of HNO_3 ($[H^+]/[Al^{3+}] = 0.1$) at 70°C for 1 h, the recrystallized sample exhibited similar crystallinity to that of the starting boehmite. However, the sample dispersed in the same solution under microwave irradiation at 70 °C for 1 h exhibited less intense and broader diffraction peaks. The latter shows that under microwave conditions, boehmite is dispersed with simultaneous amorphization of its crystallites. The ^{27}Al-NMR spectra of dispersed boehmite at 70 °C (see Figure 1S in the Supporting Information) show peaks assigned to boehmite at ∼8.9 ppm and to small monomeric and oligomeric aqueous Al^{3+} species at 0.5ppm (26).

The TG profiles (Figure 2S in the Supporting Information) show an increase in the amount of water in the dispersed boehmite samples. Catapal A has ∼22 wt % H_2O, which corresponds to $Al_2O_3 \cdot 1.6H_2O$, and can be considered a pseudoboehmite (1). After dispersion, the weight change was ∼33%, which corresponds to $Al_2O_3 \cdot 2.8H_2O$. The TG profiles (see Figure 2S in the Supporting Information) for all boehmite-P123 nanocomposites are similar, showing one broad decomposition step (∼70 wt %) in the range of 200−400°C. The composites obtained from alkoxide precursor exhibit three decomposition steps at lower temperatures.

After calcination at 400°C, all BMA samples exhibited nanocrystalline domains corresponding to different transition alumina phases (see Figure 1 caption). The samples obtained from boehmite dispersed under microwave irradiation exhibited crystallinity above 700 °C calcination. The assigned phases were the same as those for other boehmite materials. Their powder diffraction patterns (see Figure 3S in the Supporting Information) were similar to those shown in

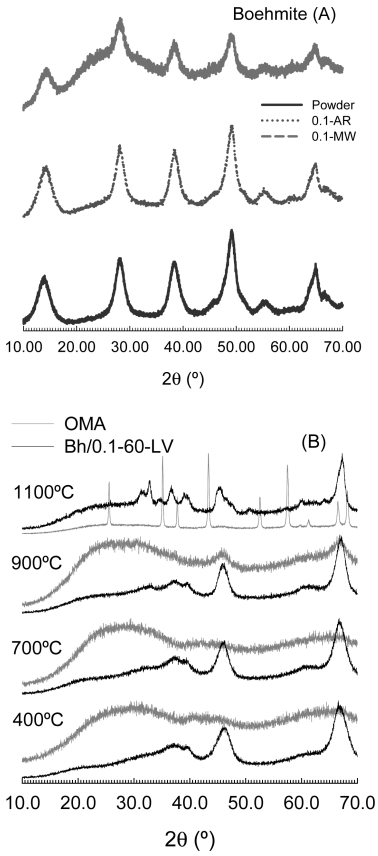

FIGURE 1. XRD patterns (A) for boehmite powder and re-crystallized boehmite after dispersion in HNO_3 aqueous solutions at 70 °C for 1 h and drying at 60 °C for 12 h using conventional (AR) and microwave (MW) conditions and (B) for the materials prepared in the presence of Pluronic P123 and calcined at different temperatures; black lines refer to the samples obtained from boehmite and grey lines refer to the samples prepared from alkoxide precursor. Assignments: (A) boehmite (JCPDS 1-774), and (B) γ-Al_2O_3 at 400 and 600 °C (JCPDS 1-1303), δ-Al_2O_3 at 900 °C (JCPDS 47-1770), and $\delta+\theta$-Al_2O_3 after calcination at 1100 °C (JCPDS 47-1770 and 23-1009, respectively) for the boehmite-generated samples, and α-Al_2O_3 for the alkoxide-derived sample (JCPDS 10-173).

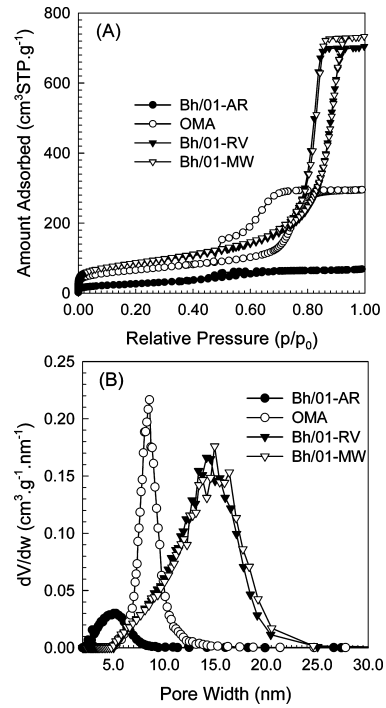

FIGURE 2. (A) Nitrogen adsorption isotherms at −196°C for the selected samples calcined at 700 °C for 4 h in flowing air and (B) the corresponding PSD curves calculated by the KJS method (24, 25).

Figure 1B for the BMA sample prepared using the low acid concentration and low volume of solvents (Bh/0.1-60-LV). The alkoxide sample, OMA, was completely amorphous until calcination at 900 °C, see Figure 1B. The latter was converted into nonporous α-Al_2O_3 after 1 h calcination at 1100 °C (see the XRD pattern for OMA in Figure 4S in the Supporting Information), whereas such conversion did not occur for the boehmite-based sample treated at 1100 °C because of kinetic effects; in this case, $\delta+\theta$-Al_2O_3 phases were identified.

Nitrogen adsorption isotherms for the BMA samples studied are type IV as shown in Figure 2A and Figure 5S in the Supporting Information. Adsorption isotherms for the OMA samples exhibit steep capillary condensation steps and H-1 hysteresis loops characteristic for uniform cylindrical mesopores. The desorption branches for the OMA samples calcined at 400 and 700 °C are stepwise and end at the limiting pressure of the hysteresis loop closure indicating the presence of some pore constrictions. The BMA samples have hysteresis loops characteristic for the materials with mesopores between aggregated small particles. The calculated pore size distribution curves, Figure 2B, confirm the uniformity of mesopores in OMA, whereas the boehmite materials have about twice larger mesopores and also broader PSDs than those for OMA. The adsorption parameters for the samples studied are summarized in Table 1 and Table 1S in the Supporting Information. These data show that the boehmite-based samples prepared in the presence of block copolymer exhibited larger pore volumes than those prepared without polymer or these obtained from alkoxide precursor (see Tables 1 and 1S in the Supporting Information).

Also, the BMA samples showed higher acidity than OMAs calcined under the same conditions (see Figure 3). This acidity was estimated by integration of the NH_3-TPD profiles shown in Figure 3 and in Figures 7S and 8S in the Suppporting Information (the acidity data are summarized in Table 1 and Table 2S in the Supporting Information). Although OMA showed similar acidity to that of the recrystallized boehmite and calcined at 700 °C, ~540 μmol of NH_3 g^{-1}; this parameter increased to ~765 μmol of NH_3 g^{-1} for Bh/0.1-60-RV/700. Also, the sample prepared from the microwave-dispersed boehmite had much higher amounts of sites than OMA/700, as a result of better crystallinity and higher specific surface area. In general, this parameter decreased for all series with increasing calcination temperature. Nevertheless, the BMA samples calcined at 1100 °C still had relatively high surface areas (at least 100 m^2 g^{-1}), exhibited transition phases, and had superior acidities in comparison to those of OMA after calcination at the same temperature.

The numbers of basic sites estimated using CO_2-TPD (see Figure 3) were also higher for the BMA samples compared to the OMA materials. For instance, these values for the

Table 1. Parameters Obtained from Nitrogen Adsorption at −196°C, and NH_3 Temperature Program Desorption (TPD) Data; Values in Parentheses were Obtained from Adsorption Isotherms for the Samples after NH_3-TPD Experiments[a]

sample (700 °C)	S_{BET} (m^2/g)	V_{SP} (cm^3/g)	w_{KJS} (nm)	n_{NH_3} (μmol/g)	ASA (m^2/g)
Bh/0.1-AR	96 (236)	0.10 (0.28)	5.28 (5.81)	538	45
Bh/0.2-60-RV	286	1.15	16.32	660	56
Bh/0.1-60-RV	308 (333)	1.08 (1.15)	14.16 (14.24)	765	64
Bh/0.1-60-MW	314 (312)	1.13 (1.15)	14.96 (15.45)	629	53
OMA	235 (186)	0.46 (0.38)	8.56 (8.83)	540	45

[a] S_{BET}, specific surface area calculated in the relative pressure range of 0.05−0.20 using the BET equation; V_{SP}, single-point pore volume calculated from the amount adsorbed at relative pressure of 0.99; w_{KJS}, pore width at the maximum of the pore size distribution (PSD) calculated by the KJS method calibrated for the 2−19 nm mesopore range (24, 25); n_{NH_3}, amount of acid sites calculated by integration of the TPD profile; ASA, active surface area obtained from n_{NH_3} by using 0.14 nm^2/molecule for the average value of the cross-sectional area of ammonia molecule (27).

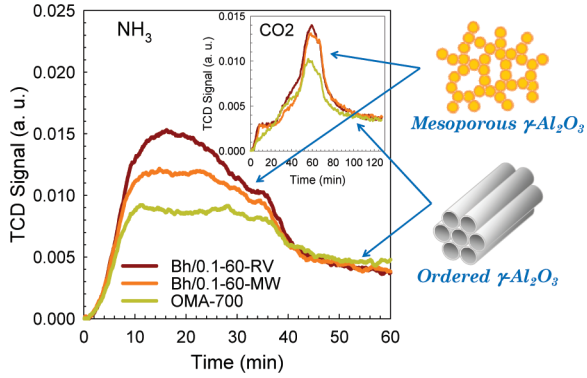

FIGURE 3. Comparison of NH_3-TPD profiles for the boehmite-based (Bh/0.1-60-RV/700 and Bh/0.1-60-MW/700) and alkoxide-based (OMA-700) alumina samples with the corresponding CO_2-TPD profiles (inset).

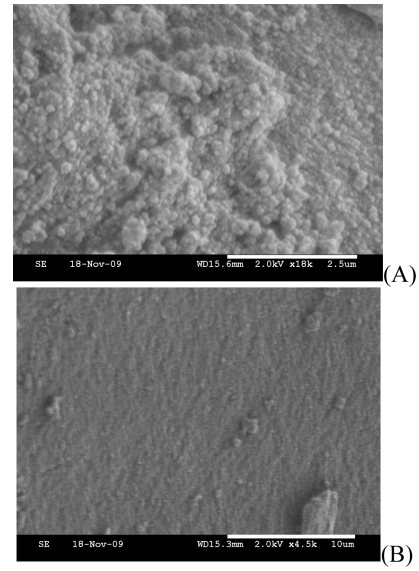

FIGURE 4. SEM images for (A) Bh/0.1-60-RV/400 and (B) Bh/0.1-60-MW/400 showing distinct morphologies for the materials obtained from boehmite dispersed under conventional (larger granules) and microwave conditions.

samples Bh/0.1-60-RV/700 and Bh/0.1-60-MW/700 are 599 and 629 μmol of CO_2 g^{-1}, respectively; they are higher than 545 μmol of CO_2 g^{-1} obtained for OMA. The strength of basic sites, estimated on the basis of maximum desorption temperature was similar for all three samples, being in the range of 630 (OMA) to 670 °C (Bh/0.1-60-RV/700).

Nitrogen adsorption isotherms and the corresponding PSDs for the samples after NH_3-TPD measurements are shown in Figure 7S in the Supporting Information; the corresponding data are listed in Table 1 and in Table 1S in the Supporting Information. Although the boehmite materials were practically unchanged after TPD measurements, the alkoxide ones exhibited lower surface area and pore volume. The recrystallized material showed larger pore volume as a result of its exposure to NH_3 and consecutive heating cycles at 500 °C. The latter results provide preliminary evidence for the better thermal and chemical stability of boehmite-based mesoporous aluminas prepared in the presence of triblock copolymers, which is highly desirable for catalytic applications.

The SEM images for the BMA materials dispersed under conventional and microwave conditions are shown in Figure 4 and Figure 9S in the Supporting Information. All synthesis gels afforded large monolithic particles that were preserved after calcinations at temperatures up to 800°C. The Bh/0.1-60-RV/400 sample shown in Figure 4A has a particle surface composed of larger alumina spherical aggregates than those in Bh/0.1-60-MW/400 (Figure 4B). These images also show distinct morphologies (see Figure 9SA−D in the Supporting Information) for the current BMA samples than those previously reported for the transition alumina phases obtained by direct dehydroxylation of crystalline boehmite and gibbsite precursors (28), or for boehmite prepared from alkoxide precursors (29). Similar alumina aggregates were reported for the BMA materials prepared after dispersing boehmite in HNO_3 solutions without the use of structure directing agents (29).

The MA materials with flowerlike and fiberlike morphologies have been prepared using hydrothermal alkaline conditions for hydrolysis of $Al_2(SO_4)_3.18H_2O$ in the presence of sodium tartrate (30) or $Al(NO_3) \cdot 9H_2O$ in the presence of P123 as structure directing agents (31), respectively. Although the former work shows the time-dependent formation of spherical boehmite particles and their transformation into hollow particles via partial AlOOH dissolution, the latter shows the effect of boehmite dispersion under hydrothermal conditions in the presence of triblock copolymers for the preferential growth of fibers. The present synthesis performed under acidic conditions with slow evaporation fa-

Scheme 1. Proposed Mechanism for the Formation of Mesoporous Alumina from Boehmite in the Presence of Block Copolymer: (1) Dispersion of Boehmite Powder in Slightly Acidic Aqueous Solution, (2) Interaction of Block Copolymer with Species Formed during Boehmite Dispersion, (3) Formation of Polymer−Alumina Mesostructured Composite, and (4) Removal of Polymer from the aforementioned Composite

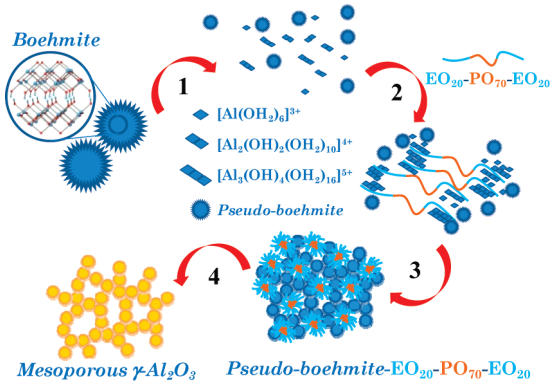

vored growth of particles in 3D and without a preferred orientation, such as fibers or platelets.

The previously proposed mechanism of formation of the BMA materials assumed the block copolymer-assisted agglomeration of boehmite-generated species into sandwich-type structures (19, 21, 31), whereas the hydrothermal synthesis of MA by alkaline hydrolysis of $AlCl_3$ in the presence of sodium polyacrylate also afforded samples with fiberlike morphology, which was explained on the basis of the time-dependent orientation effects of a nematic phase formed by polyacrylate with a charge balance effect between the positively charged sodium ions and the negatively charged pseudo-boehmite framework.

However, none of the previous studies using triblock copolymers accounted for the formation of nearly spherical aggregates as building units for much larger 3D monolithic BMA structures. Thus, we propose that after formation of layered-type structures involving small oligomeric aluminum species identified by ^{27}Al-NMR and triblock copolymers, these aqueous species provide connectivity between larger pseudo-boehmite nanoparticles formed in solution (see ^{27}Al-NMR in Figure 1S in the Supporting Information and the mechanism shown in Scheme 1). The 3D pseudo-boehmite-triblock copolymer superstructure grows by agglomeration of the spherical particles, resulting in materials with thicker pore walls and better crystallinity.

Also, boehmite dispersed under microwave irradiation exhibits smaller crystallite sizes than those dispersed under conventional hydrothermal conditions. These gels afforded materials composed of smaller spherical BMA particles and consequently smoother surfaces. Thus, this finding shows some possibilities for the control of the size of BMA particles after self-assembly with P123 and the crystallinity of the final materials. Although materials prepared under conventional conditions exhibited higher number of acid sites than amorphous OMA and the microwave-assisted samples, the latter exhibited the slightly higher number of basic sites.

CONCLUSIONS

The use of dispersed boehmite in acidified aqueous solution in the synthesis of MA in the presence of triblock copolymer afforded the BMA samples with large mesopores, large pore volume, high surface area, high crystallinity, greater acidity, and better thermal stability than the soft-templated MA samples obtained from alkoxide precursor and the other alumina samples prepared without polymer templates. Porosity of the BMA materials is comparable to that of alumina aerogels (32). The presence of large mesopores in the BMA samples can be beneficial for catalytic applications such as Fischer−Tropsch synthesis, where large pore alumina-supported catalysts are preferred (33). This study also clarifies the mechanism of formation of the BMA materials, which involves the block copolymer-assisted agglomeration of boehmite-generated species into sandwich-type structures as illustrated in Scheme 1 (19, 21). In addition, these species provide connectivity for the formation of larger pseudo-boehmite nanoparticles in solution, resulting in much more stable BMA materials after template removal.

Most importantly, the BMA samples from boehmite dispersions prepared under conventional and microwave conditions exhibited similar specific surface areas and the same transition alumina phases after calcination ≥700 °C. However, the number of acid and basic sites between the two sets of samples was different, showing that it is possible to tailor the surface properties of alumina materials by using the same starting reagents, without additives and pH adjustments. These results are of great importance for the future applications of MA as catalysts, supports (1−3, 34−36), and membranes (37) for which numbers and types of acid and basic sites are directly linked to the activity of the MA materials (36) and to their interactions with metal catalysts (34, 35, 38). Although these properties are directly linked to the transition alumina phases, the transition from an amorphous into a crystalline material with the defective spinel structure ensures the types of aluminum sites and vacancies associated with the desired surface acidity and catalytic activity (34).

Acknowledgment. This work was partially supported by the National Science Foundation under Grant CHE-0649017 (REU); R.I.B., an undergraduate student from Kent State University (KSU), participated in the REU 2009 summer program at KSU.

Supporting Information Available: Tables 1S and 2S with adsorption and NH_3-TPD parameters, Figures 1S−9S containing N_2 adsorption isotherms at −196°C, the PSD curves, powder XRD patterns, NH_3-TPD profiles, and SEM images for the MA samples studied (PDF). This material is available free of charge via the Internet at http://pubs.acs.org.

REFERENCES AND NOTES

(1) Oberlander, R. K. In *Applied Industrial Catalysis*; Leach, B. E., Ed.; Academic Press:London, 1984; pp 397.

(2) Pinnavaia, T. J.; Zhang, Z. R.; Hicks, R. W. In *Nanoporous Materials*; Sayari, A., Jaroniec, M., Eds.; World Scientific: Singapore, 2005; pp 1−10.
(3) Márquez-Alvarez, C.; Žeilková, N.; Pérez-Pariente, J.; Čejka, J. *Catal. Rev.−Sci. Eng.* **2008**, *50*, 222–286.
(4) Čejka, J. *Appl. Catal., A* **2003**, *254*, 327–338.
(5) Yang, P.; Zhao, D.; Margolese, D.; Chmelka, B.; Stucky, G. *Nature* **1998**, *396*, 152–155.
(6) Niesz, K.; Yang, P.; Somorjai, G. A. *Chem. Commun.* **2005**, *2005*, 1986–1987.
(7) Liu, Q.; Wang, A.; Wang, X.; Zhang, T. *Chem. Mater.* **2006**, *18*, 5153–5155.
(8) Yuan, Q.; Yin, A.; Luo, C.; Sun, L.; Zhang, Y.; Duan, W.; Liu, H.; Yan, C. *J. Am. Chem. Soc.* **2008**, *130*, 3465–3472.
(9) Morris, S. M.; Fulvio, P. F.; Jaroniec, M. *J. Am. Chem. Soc.* **2008**, *130*, 15210–15216.
(10) Li, L.; Duan, W.; Yuan, Q.; Li, Z.; Duan, H.; Yan, C. *Chem. Commun.* **2009**, 6174–6176.
(11) Kuemmel, M.; Grosso, D.; Boissière, C.; Smarsly, B.; Brezesinski, T.; Albouy, P. A.; Amenitsch, H.; Sanchez, C. *Angew. Chem., Int. Ed.* **2005**, *44*, 4589–4592.
(12) Wan, L.; Fu, H.; Shi, K.; Tian, X. *Mater. Lett.* **2008**, *62*, 1525–1527.
(13) Wang, L.; Yang, R. T. *J. Phys. Chem. C* **2008**, *112*, 12486–12494.
(14) Caragheorgheopol, A.; Caldararu, H.; Ionita, G.; Savonea, F.; Žilková, N.; Zukal, A.; Cejka, J. *Langmuir* **2005**, *21*, 2591–2597.
(15) Zhang, Z.; Pinnavaia, T. J. *Angew. Chem., Int. Ed.* **2008**, *47*, 7501–7504.
(16) Hicks, R. W.; Castagnola, N. B.; Zhang, Z.; Pinnavaia, T. J.; Marshall, C. L. *Appl. Catal. A* **2003**, *254*, 311–317.
(17) Zhang, Z.; Hicks, R. W.; Pauly, T. R.; Pinnavaia, T. J. *J. Am. Chem. Soc.* **2002**, *124*, 1592–1593.
(18) Ren, T.; Yuan, Z.; Su, B. *Langmuir* **2004**, *20*, 1531–1534.
(19) González-Peña, V.; Díaz, I.; Márquez-Alvarez, C.; Sastre, E.; Pérez-Pariente, J. *Microporous Mesoporous Mater.* **2001**, *44−45*, 203–210.
(20) Valange, S.; Guth, J.; Kolenda, F.; Lacombe, S.; Gabelica, Z. *Microporous Mesoporous Mater.* **2000**, *35−36*, 597–607.
(21) Liu, Q.; Wang, A.; Wang, X.; Gao, P.; Wang, X.; Zhang, T. *Microporous Mesoporous Mater.* **2008**, *111*, 323–333.
(22) Liu, Q.; Wang, A.; Wang, X.; Zhang, T. *Microporous Mesoporous Mater.* **2006**, *92*, 10–21.
(23) Kruk, M.; Jaroniec, M. *Chem. Mater.* **2001**, *13*, 3169–3183.
(24) Kruk, M.; Jaroniec, M.; Sayari, A. *Langmuir* **1997**, *13*, 6267–6273.
(25) Jaroniec, M.; Solovyov, L. A. *Langmuir* **2006**, *22*, 6757–6760.
(26) Morgado, E., Jr.; Lam, Y. L.; Menezes, S. M. C.; Nazar, L. F. *J. Colloid Interface Sci.* **1995**, *176*, 432–441.
(27) McClellan, A. L.; Harnsberger, H. F. *J. Colloid Interface Sci.* **1967**, *23*, 577–599.
(28) Santos, P. S.; Santos, H. S.; Toledo, S. P. *Mater. Res.* **2000**, *3*, 104–114.
(29) Zhang, X.; Honkanen, M.; Levänen, E.; Mäntylä, T. *J. Cryst. Growth* **2008**, *310*, 3674–3679.
(30) Cai, W.; Yu, J.; Cheng, B.; Su, B.; Jaroniec, M. *J. Phys. Chem. C* **2009**, *113*, 14739–14746.
(31) Bai, P.; Su, F.; Wu, P.; Wang, L.; Lee, F. Y.; Lv, L.; Yan, Z.; Zhao, X. S. *Langmuir* **2007**, *23*, 4599–4605.
(32) Baumann, T. F.; Gash, A. E.; Chinn, S. C.; Sawvel, A. M.; Maxwell, R. S.; Satcher, J. H. *Chem. Mater.* **2005**, *17*, 395–401.
(33) Lesaint, C.; Kleppa, G.; Arla, D.; Glomm, W. R.; Oye, G. *Microporous Mesoporous Mater.* **2009**, *119*, 245–251.
(34) Trueba, M.; Trasatti, S. P. E. J. *Inorg. Chem.* **2005**, *2005*, 3393–3403.
(35) Dandapat, A.; Jana, D.; De, G. *ACS Appl. Mater. Interfaces* **2009**, *1*, 833–840.
(36) Carre, S.; Gnep, N. S.; Revel, R.; Magnoux, P. *Appl. Catal., A* **2008**, *348*, 71–78.
(37) Lin, Y. S. *Sep. Purif. Technol.* **2001**, *25*, 39–55.
(38) Kwak, J. H.; Hu, J.; Mei, D.; Yi, C.; Kim, D. H.; Peden, C. H. F.; Allard, L. F.; Szanyi, J. *Science* **2009**, *325*, 1670–1673.

AM9009023